to appear in Applied Mathematics and Computations

Approximate stability charts for milling processes using semi-discretization

Ferenc Hartung [*], Tamás Insperger[†], Gábor Stépán[‡], Janos Turi[§]

Keywords: delay-differential equations, preservation of stability, semi-discretization, machine tool chatter, approximation of stability charts

Abstract

Unwanted relative vibrations between the tool and the workpiece represent significant challenges in high-speed machining. In order to avoid this problem, one needs to specify ranges for system parameters (spindle speed, depth of cut) for which the process is stable, i.e., to obtain a so-called stability chart. Such stability charts usually can only be given by numerical means which is illustrated in the paper for a single degree of freedom model of milling. In this paper, we establish the convergence of the semi-discretization approximation method for a class of delay equations modeling the milling process. Moreover, we show that semi-discretization preserves asymptotic stability of the original equation, thus it can be used to obtain good approximations for the stability charts.

1 Introduction

It has been known for a long time, that past effects need to be included in the modeling of certain dynamic problems. One of the classical examples is the predator-prey model of Volterra [1], where the growth rate of predators depends not only on the present

[*]Department of Mathematics and Computing, University of Veszprém, H-8201 Veszprém, POB 158, Egyetem u. 10., Hungary, phone: 36-88-423239, fax: 36-88-421-693, e-mail: hartung@szt.vein.hu

[†]Department of Applied Mechanics, Budapest University of Technology and Economics, H-1521 Budapest, Hungary, phone: 36-01-463-1227, fax: 36-01-463-3471, e-mail: inspi@mm.bme.hu

[‡]Department of Applied Mechanics, Budapest University of Technology and Economics, H-1521 Budapest, Hungary, phone: 36-01-463-1369, fax: 36-01-463-3471, e-mail: stepan@mm.bme.hu

[§]Programs in Mathematical Sciences, University of Texas at Dallas, Richardson, TX 75083, phone: (972)-883-2183, fax: (972)-883-6622, e-mail: turi@utdallas.edu

quality of food (say, prey), but also on the past quantities (say, in the period of gestation). The first delay models in engineering appeared for wheel shimmy [2], and for ship stabilization [3]. There are several other problems in engineering, where time delays arise, like in the modeling of machine tool vibrations in cutting processes [4,5], in robotics telemanipulation with transport delay [6], or in neural network models, where the interactions of the neurons are delayed [7]. Qualitative and quantitative analysis of delayed systems is therefore an important issue in many applications.

A numerical technique, the so-called semi-discretization was used in [8] to obtain approximate solutions for retarded functional differential equations (RFDEs). The essence of the method is that the delayed and the time dependent terms are approximated by piecewise constant values (zeroth order approximation), and, consequently, the RFDE is approximated by a series of ordinary differential equations (ODEs). The solutions of these ODEs lead to a finite dimensional discrete map approximation of the RFDE. The semi-discretization method can effectively be used for analysing cutting processes, like the milling process for which the governing RFDE has time periodic coefficients [5], the turning process with varying spindle speed for which the time delay itself is also time dependent in the governing RFDE [9], or feedback control systems [10, 11]. We note that the method was recently refined in [12] and [13].

The main goal of this paper is to provide a convergence proof for the semi-discretization method for a class of RFDEs which appear in engineering applications. It will be also shown, using a perturbation argument, that the semi-discretization method can be used to construct approximate stability charts for these applications.

In particular, we investigate linear, T-periodic, RFDEs of the form

$$\dot{\mathbf{x}}(t) = \mathbf{A}(t)\mathbf{x}(t) + \sum_{j=1}^{r} \mathbf{R}_j(t)\mathbf{x}(t-\tau_j) + \int_{-\sigma}^{0} \mathbf{W}(\vartheta,t)\mathbf{x}(t+\vartheta)\mathrm{d}\vartheta\,, \tag{1}$$

$$\mathbf{A}(t+T) = \mathbf{A}(t), \quad \mathbf{R}_j(t+T) = \mathbf{R}_j(t), (j=1,\ldots,r), \quad \mathbf{W}(\vartheta,t+T) = \mathbf{W}(\vartheta,t)\,,$$

where $\mathbf{A}(t)$, $\mathbf{R}_j(t)$ and $\mathbf{W}(\vartheta,t)$ are matrix valued functions.

In the present investigation, it is assumed that the matrices $\mathbf{A}(t)$ and $\mathbf{W}(\vartheta,t)$ have discontinuities in t. These discontinuities arise in the mechanical model: during the milling process, the number of working teeth are changing corresponding to the entry and exit of the teeth into and from the cut.

The rest of the paper is organized as follows. In Section 2, we provide an example: numerical simulations using semi- and full-discretization for constructing approximate stability charts for a single degree of freedom milling model. In Section 3, we present theoretical results for convergence of approximations and preservation of asymptotic stability under approximation for a class of delay-differential equations using the so-called semi-discretization method.

2 Motivation: stability analysis of the milling process

In engineering problems, stability properties of dynamical systems are usually demonstrated by stability charts. These charts present the parameter values for which the system is stable or unstable. The current investigation was motivated by the analysis of the milling process. For milling, stability charts are given in the parameter plane of the spindle speed and the depth of cut. Accurate modeling of both the regenerative and the tooth pass excitation effects in milling results in an RFDE with periodically varying coefficients. In [8, 5], the semi-discretization method was used to create stability charts for RFDE's modeling the milling process.

2.1 A model of the milling process

Dynamical models of the milling process assume that either the tool or the workpiece or both of them are flexible, and due to the exciting effect of the cutting force, vibrations may arise. There are two essential phenomena in the milling process that characterize its dynamics. One is the regenerative effect: the tool cuts the surface that was formed by the previous tooth pass, therefore the chip thickness, and consequently the cutting force depends on the actual tool position and the position one tooth pass earlier. Second is the tooth passing excitation effect: since the tool is rotating and the teeth periodically enter and leave the cut, the cutting force is a time periodic function of time with period equal to the tooth passing period. Accurate modeling of both effects leads to a time periodic RFDE.

In the following preliminary example, we investigate the equation of a single degree of freedom milling model (see [5] for details):

$$\ddot{x}(t) + 2\zeta\omega_n\dot{x}(t) + \omega_n^2 x(t) = \frac{bK(t)}{M}\left(x(t-\tau) - x(t)\right) . \tag{2}$$

The left-hand side of the equation is associated to the single degree of freedom damped oscillator, the term in right-hand side comes from the cutting force. The time delay in (2) is equal to the tooth passing period: $\tau = 60/(N\Omega)$, where Ω is the spindle speed given in [rpm] and N is the number of teeth. The periodic function $K(t) = K(t+\tau)$ reads

$$K(t) = \sum_{p=1}^{N} \left\{ g_p(t) \left(K_t \cos\left(\frac{2\pi\Omega}{60}t + p\frac{2\pi}{N}\right) + K_n \sin\left(\frac{2\pi\Omega}{60}t + p\frac{2\pi}{N}\right)\right) \right. \\ \left. \times \sin\left(\frac{2\pi\Omega}{60}t + p\frac{2\pi}{N}\right)\right\} . \tag{3}$$

The function $g_p(t)$ determines if the tooth denoted by p is cutting or not:

$$g_p(t) = \begin{cases} 1 & \text{if} \quad \varphi_{enter} < \varphi_p < \varphi_{exit} \\ 0 & \text{otherwise} \end{cases} , \tag{4}$$

where φ_{enter} and φ_{exit} are the angles where the teeth enter and exit the cut, respectively (see Figure 1).

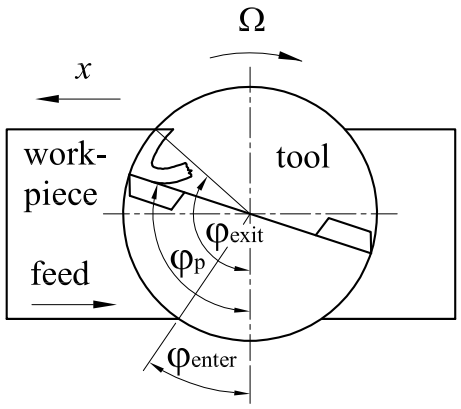

Figure 1: Modeling the entering end exiting teeth in the milling process

All the other parameters are summarized in Table 1. For these parameters, the graph of function $K(t)$ is shown in Figure 2. The discontinuity of the function is due to the tooth passing effect. In the present case the number of teeth is 2, and the enter and exit angles are 0° and 150°, respectively. If the angular position of the teeth are $150° < \varphi_1 < 180°$ and $330° < \varphi_2 < 360°$, then both teeth are out of cut and the function $K(t)$ is zero.

natural frequency	$\omega_n = 920.5$ rad/s
relative damping	$\zeta = 0.0032$
modal mass	$M = 2.573$ kg
tangential cutting coefficient	$K_t = 5.5 \times 10^8$ N/m^2
normal cutting coefficient	$K_n = 2 \times 10^8$ N/m^2
number of teeth	$N = 2$
tooth enter angle	$\varphi_{enter} = 0°$
tooth exit angle	$\varphi_{exit} = 150°$
depth of cut	$b = 1$ mm
spindle speed	$\Omega = 9000$ rpm

Table 1: Parameters for milling process

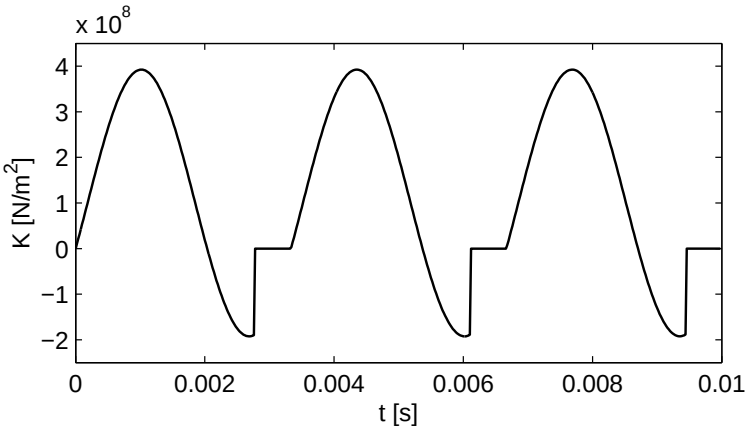

Figure 2: Graph of $K(t)$

2.2 Comparison of semi-discretized and fully-discretized simulations

In [8, 5], semi-discretization was used to construct stability charts corresponding to (2). However, the method can be used for simulating the solutions of RFDEs, as well. Piecewise constant approximation of the delayed term $x(t-\tau)$ and the time dependent coefficient $K(t)$ in (2) leads to the semi-discretized equation

$$\ddot{x}(t) + 2\zeta\omega_n\dot{x}(t) + \left(\omega_n^2 + \frac{bK_i}{m}\right)x(t) = \frac{bK_i}{m}x_{i-m}\,, \quad t \in [ih, (i+1)h]\,, \quad i \in \mathbb{Z} \tag{5}$$

where

$$K_i = \int_{ih}^{(i+1)h} K(s)ds\,, \tag{6}$$

$x_{i-m} = x((i-m)h)$ and $h = \tau/m$, $m \in \mathbb{Z}$. Here, m is an approximation parameter, it defines the number of discretization steps over a time interval of length τ.

For initial conditions $x(ih) = x_i$, $\dot{x}(ih) = v_i$ and for a known x_{i-m}, (5) can be solved for each discretization step as an ordinary differential equation. The displacement and the velocity for the next discretization step can be expressed as the linear combination of the discrete values x_i, v_i, x_{i-m}:

$$x((i+1)h) = x_{i+1} = a_{1,i}x_i + a_{2,i}v_i + a_{3,i}x_{i-m}\,, \tag{7}$$

$$\dot{x}((i+1)h) = v_{i+1} = a_{4,i}x_i + a_{5,i}v_i + a_{6,i}x_{i-m}\,, \tag{8}$$

where the coefficients $a_{k,i}$ ($k = 1, \ldots, 6$, $i \in \mathbb{Z}$) can be computed using the parameters summarized in Table 1 (for details, see [8, 5]). If the initial values x_i, x_{i-1}, ..., x_{i-m} and v_i are given, then the semi-discretized solution can be continued in the subsequent discretization steps (semi-discretized simulation).

The step-by-step solution of (5) is presented in Figure 3 for different approximation parameters m. The initial condition was chosen to be $x_i = x_{i-1} = x_{i-2} = \cdots = x_{i-m} = 10^{-4}$ [m] for the actual and the delayed displacements and $v_i = 0$ for the velocity. This initial condition corresponds to a reasonable perturbation around the $x \equiv 0$ solution. The parameters are given in Table 1. Note, that the spindle speed Ω and the depth of cut b parameters were set so that the system is close to the boundary of stability (see Figure 5). Consequently, the solution is an almost periodic function. Figure 3 indicates the convergence of the semi-discretized solutions.

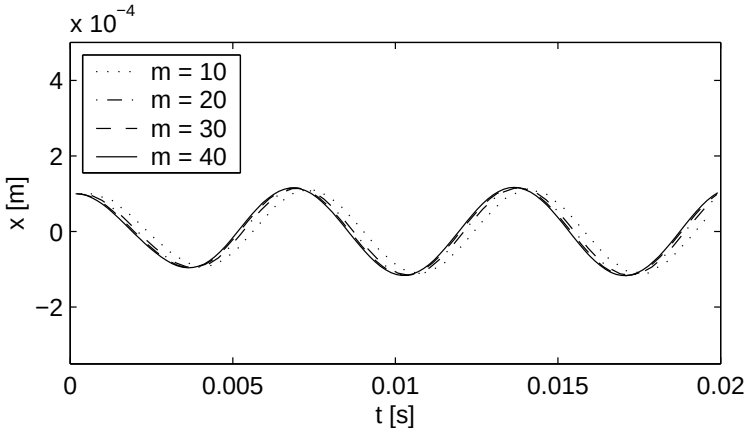

Figure 3: Semi-discretized simulation for (2) with different step sizes

The main difference in semi-discretization, as opposed to the traditional full-discretization, is that only the delayed states and the time dependent coefficients are discretized. In order to see the difference between semi- and full-discretization, (2) is also solved by using full-discretization. The derivatives are approximated as:

$$\dot{x}(t) \approx \frac{x_{i+1} - x_i}{h}\,, \tag{9}$$

$$\ddot{x}(t) \approx \frac{x_{i+2} - 2x_{i+1} + x_i}{h^2}\,, \tag{10}$$

where $x_i = x(ih)$, again. The fully-discretized equation reads

$$\frac{x_{i+2} - 2x_{i+1} + x_i}{h^2} + 2\zeta\omega_n \frac{x_{i+1} - x_i}{h} + \omega_n^2 x_i = \frac{bK_i}{m}(x_{i-m} - x_i)\,. \tag{11}$$

Here, x_{i+2} can be expressed as the linear combination of x_{i+1}, x_i and x_{i-m}:

$$x_{i+2} = b_1 x_{i+1} + b_{2,i} x_i + b_{3,i} x_{i-m}\,, \tag{12}$$

where $b_1 = 2(1 - h\zeta\omega_n)$, $b_{2,i} = 2h\zeta\omega_n - \left(\omega_n^2 + \frac{bK_i}{m}\right) h^2 - 1$ and $b_{3,i} = \frac{bK_i}{m} h^2$. If the initial values x_{i+1}, x_i, $\ldots$, x_{i-m} are given, then the fully-discretized solution can be continued in the subsequent discretization steps (fully-discretized simulation). The convergence

of the fully-discretized scheme for linear and later for general RFDEs with time- and state-dependent delays was proved in [14, 15].

For computations, the same reasonable initial condition was chosen as for the semi-discretization: $x_i = 10^{-4}$ m, $v_i \approx (x_{i+1} - x_i)/h = 0$, $x_{i-2} = x_{i-3} = \cdots = x_{i-m} = 10^{-4}$ [m]. The solution obtained by full-discretization can be seen in Figure 4. It can be seen that the solutions converge to the almost periodic function as the semi-discretized simulations does in Figure 3, but the convergence is much slower than that of semi-discretization. Here, approximation parameter $m = 500$ should be used to obtain acceptable result.

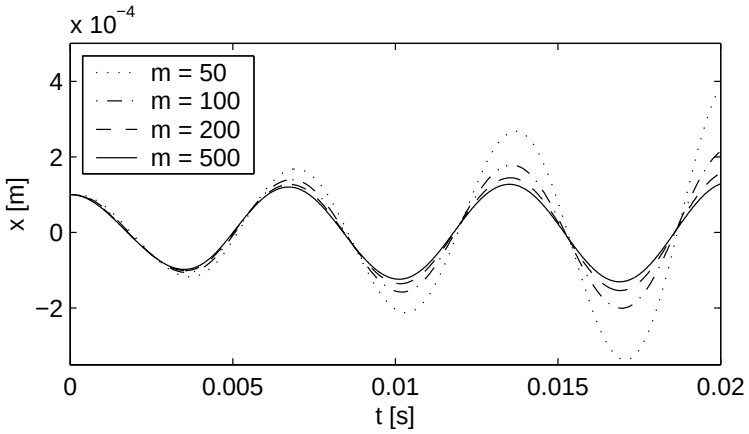

Figure 4: Fully-discretized simulation for (2) for different step sizes

2.3 Comparison of stability charts obtained by semi- and full-discretization

To construct stability charts, values for parameters Ω and b should be found so that the system is stable. Therefore, in this section, the parameters Ω and b are not fixed, they are considered as independent variables (all the other parameters are fixed according to Table 1).

For stability analysis of (2) by semi-discretization, the same stepwise solution is used as in equations (7) and (8), but now, the coefficients depend on the parameters Ω and b: $a_{k,i} = a_{k,i}(\Omega, b)$, $k = 1, \ldots, 6$, $i \in \mathbb{Z}$. This stepwise solution provides the discrete map

$$\mathbf{y}_{i+1} = \mathbf{B}_i(\Omega, b)\mathbf{y}_i\,, \tag{13}$$

where the $m + 2$ dimensional state vector is

$$\mathbf{y}_i = \mathrm{col}(v_i \;\; x_i \;\; x_{i-1} \;\; \ldots \;\; x_{i-m})\,, \tag{14}$$

and the coefficient matrix has the form

$$\mathbf{B}_i(\Omega,b)=\begin{pmatrix} a_{5,i}(\Omega,b) & a_{4,i}(\Omega,b) & 0 & 0 & \dots & 0 & a_{6,i}(\Omega,b)\\ a_{2,i}(\Omega,b) & a_{1,i}(\Omega,b) & 0 & 0 & \dots & 0 & a_{3,i}(\Omega,b)\\ 0 & 1 & 0 & 0 & \dots & 0 & 0\\ 0 & 0 & 1 & 0 & \dots & 0 & 0\\ \vdots & \vdots & \vdots & \vdots & \ddots & \vdots & \vdots\\ 0 & 0 & 0 & 0 & \dots & 0 & 0\\ 0 & 0 & 0 & 0 & \dots & 1 & 0 \end{pmatrix}. \tag{15}$$

Apply (13) over the principal period $\tau = mh$ to obtain the transition matrix

$$\mathbf{\Phi}_s(\Omega,b)=\mathbf{B}_{m-1}(\Omega,b)\mathbf{B}_{m-2}(\Omega,b)\dots\mathbf{B}_0(\Omega,b)\,. \tag{16}$$

This matrix gives the connection between $\mathbf{y}_0$ and $\mathbf{y}_m$: $\mathbf{y}_m = \mathbf{\Phi}_s(\Omega,b)\mathbf{y}_0$. It is a finite, $(m+2)$ dimensional, approximation of the infinite dimensional monodromy operator of (2). If the eigenvalues of $\mathbf{\Phi}_s(\Omega,b)$ are in modulus less than 1, then the discrete map, consequently, the semi-discretized solution is asymptotically stable [16]. For any Ω and b, the transition matrix can be determined, and its eigenvalues can be evaluated. Stability charts are constructed by computing the critical eigenvalues for a set of fixed spindle speeds Ω and depth of cuts b.

Semi-discretized stability charts are presented in Figure 5 for different approximation parameters m. It can be seen that as the parameter m is increased, that is, as the step-size h is decreased, the stability boundaries converge. Even, for $m = 20$, the accuracy of the boundaries are acceptable from the engineering view of point.

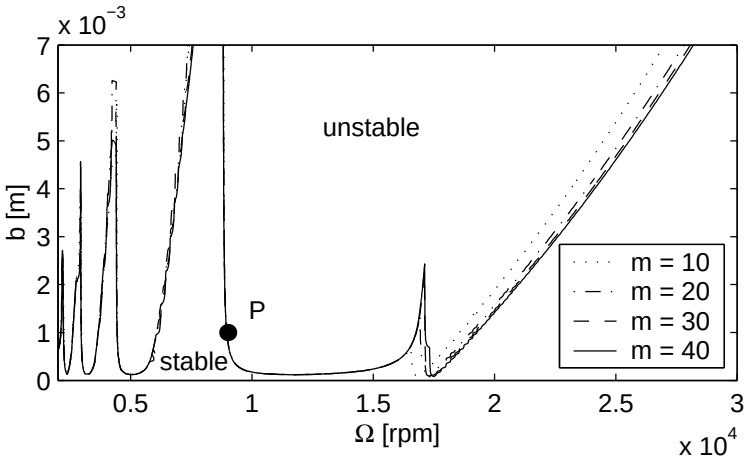

Figure 5: Semi-discretized stability charts for (2) for different step sizes

The parameter values $\Omega = 9000$ [rpm] and $b = 10^{-4}$ [m] represent the coordinates of the P in Figure 5. These parameter values were used for the simulations in the previous section. As it can be seen, this point is really close to the stability boundary.

For comparison, the same stability charts are determined by full-discretization technique. If the coefficients in (12) are considered to be dependent on the parameters Ω and b: $b_1 = b_1(\Omega, b)$ and $b_{k,i} = b_{k,i}(\Omega, b)$, $k = 2, 3$, $i \in \mathbb{Z}$, then the fully-discretized solution determines the discrete map

$$\mathbf{z}_{i+1} = \mathbf{C}_i(\Omega, b)\mathbf{z}_i \,, \tag{17}$$

where the $m + 2$ dimensional state vector is

$$\mathbf{z}_i = \mathrm{col}(x_{i+1} \;\; x_i \;\; \dots \;\; x_{i-m}) \,, \tag{18}$$

and the coefficient matrix has the form

$$\mathbf{C}_i(\Omega, b) = \begin{pmatrix} b_1(\Omega,b) & b_{2,i}(\Omega,b) & 0 & 0 & \dots & 0 & b_{3,i}(\Omega,b) \\ 1 & 0 & 0 & 0 & \dots & 0 & 0 \\ 0 & 1 & 0 & 0 & \dots & 0 & 0 \\ 0 & 0 & 1 & 0 & \dots & 0 & 0 \\ \vdots & \vdots & \vdots & \vdots & \ddots & \vdots & \vdots \\ 0 & 0 & 0 & 0 & \dots & 0 & 0 \\ 0 & 0 & 0 & 0 & \dots & 1 & 0 \end{pmatrix} . \tag{19}$$

Here, the transition matrix is obtained as

$$\mathbf{\Phi}_f(\Omega, b) = \mathbf{C}_{m-1}(\Omega, b)\mathbf{C}_{m-2}(\Omega, b) \dots \mathbf{C}_0(\Omega, b) \,. \tag{20}$$

This matrix is also a finite, $(m + 2)$ dimensional, approximation of the infinite dimensional monodromy operator. Stability analysis can be done by eigenvalue analysis of the matrix $\mathbf{\Phi}_f(\Omega, b)$, again.

Fully-discretized stability charts are presented in Figure 6 for different approximation parameters m. It can be seen that the approximation parameters are much larger and the boundaries converge much slower than in the semi-discretized charts in Figure 5. For $m = 500$, the infinite dimensional system is approximated by a 502 dimensional one, but the stability boundaries are still not accurate enough comparing to the charts obtained by semi-discretization.

Point P associated to the parameters $\Omega = 9000$ [rpm] and $b = 10^{-4}$ [m] is also presented in Figure 6. It can be seen that even for the case $m = 500$, point P is in the unstable domain, although, according to the stability chart determined by semi-discretization, point P is close to the stability boundary.

In Table 2, computation times are shown corresponding to the stability boundaries in Figures 5 and 6. The critical eigenvalues were evaluated over 100×100 number of discrete spindle speed and depth of cut values. As it can be seen, the computation times

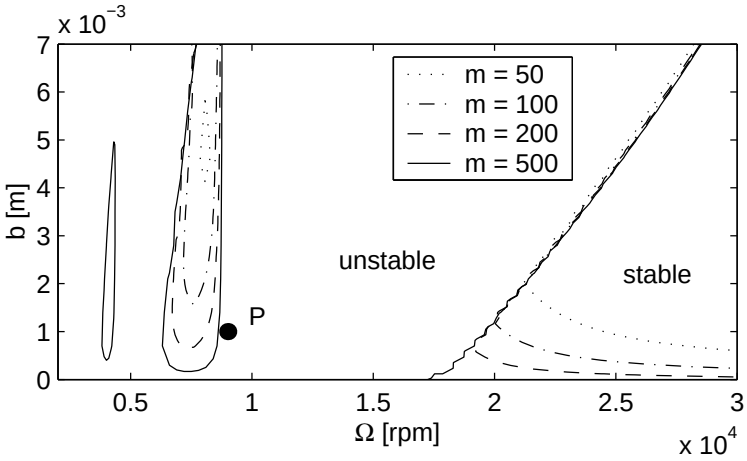

Figure 6: Fully-discretized stability charts for (2) for different step sizes

for semi-discretization are significantly shorter than those for full-discretization. For full-discretization with approximation parameter $m = 500$, the computation takes more than 12 days, and the accuracy is still poor. Comparison to the chart obtained by the semi-discretization with $m = 40$ and the corresponding 2.33 minutes of computation time shows that the semi-discretization method is much more effective than the full-discretization technique.

	semi-discretization		full-discretization
$m = 10$	0.24 min	$m = 50$	2.69 min
$m = 20$	0.58 min	$m = 100$	35.00 min
$m = 30$	1.21 min	$m = 200$	8 h 43.40 min
$m = 40$	2.33 min	$m = 500$	307 h 0.47 min

Table 2: Computation times for the stability charts determined by semi- and full-discretization in Figures 5 and 6

In the remaining part of the paper, the a mathematical analysis of the semi-discretization technique is presented including the proof of convergence of the solutions and the preservation of asymptotic stability under semi-discretization.

3 Analysis of the semi-discretization method

In this section, we consider a class of delay differential equations which includes equations proposed as mathematical models of the milling process. We introduce an associated discretized equation by applying the method of semi-discretization, and we

establish the convergence of the method for this class of equations. Finally, we show that asymptotic stability is preserved under approximations.

3.1 Notations and Preliminary Results

We say a function $g\colon [0,\infty) \to X$ (where $X = \mathbb{R}$, $\mathbb{R}^n$ or $\mathbb{R}^{n\times n}$) is piecewise-continuous, if for any finite $A > 0$, g is continuous on $[0, A]$ except possibly at finitely many $t_1, \ldots, t_m$, where finite one-sided limits exist. The set of all piecewise-continuous functions over $[0,\infty)$ is denoted by $PC([0,\infty), X)$.

We denote a fixed vector norm and the corresponding matrix norm on $\mathbb{R}^n$ and $\mathbb{R}^{n\times n}$, respectively, by $|\cdot|$.

Fix a positive constant h. We introduce the notation

$$[t]_h := \left[\frac{t}{h}\right] h$$

where $[\cdot]$ denotes the greatest integer part function. This function is piecewise constant, and it is right-continuous at the mesh points kh, $(k = 0, \pm1, \pm2, \ldots)$. Clearly, $t - h < [t]_h \le t$, hence

$$\lim_{h\to 0+} \max_{t\in\mathbb{R}} |[t]_h - t| = 0.$$

We introduce the notation

$$\langle t\rangle_h := [t]_h + \frac{h}{2}.$$

Its graph can be seen in Figure 7. Since

$$t - \frac{h}{2} < \langle t\rangle_h \le t + \frac{h}{2},$$

we have

$$\lim_{h\to 0+} \max_{t\in\mathbb{R}} |\langle t\rangle_h - t| = 0. \tag{21}$$

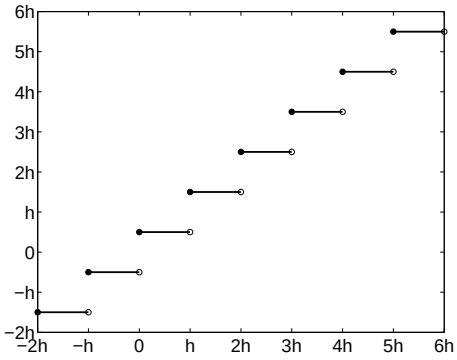

Figure 7: The graph of $\langle t\rangle_h$

For a function $\mathbf{G} \in PC([0,\infty),\mathbb{R}^{n\times n})$ we define

$$\mathcal{P}_h\mathbf{G}\colon\ [0,\infty) \to \mathbb{R}^{n\times n}, \qquad (\mathcal{P}_h\mathbf{G})(t) := \frac{1}{h}\int_{[t]_h}^{[t]_h+h} \mathbf{G}(s)\,ds. \tag{22}$$

This operator $\mathcal{P}_h$ has the following properties:

Lemma 1 *Let $\mathbf{G} \in PC([0,\infty),\mathbb{R}^{n\times n})$. Then*

(i) for any $t \geq 0$

$$\limsup_{h\to 0+} |(\mathcal{P}_h\mathbf{G})(t) - \mathbf{G}(t)| \leq |\mathbf{G}(t-) - \mathbf{G}(t)| + |\mathbf{G}(t+) - \mathbf{G}(t)|;$$

(ii) $\mathcal{P}_h\mathbf{G} \in PC([0,\infty),\mathbb{R}^{n\times n})$;

(iii) if $|\mathbf{G}(t)| \leq K$ for $t \geq 0$, then $|(\mathcal{P}_h\mathbf{G})(t)| \leq K$ for $t \geq 0$.

Proof If $\mathbf{G}$ is continuous at t, then there exists a neigbourhood of t where $\mathbf{G}$ is uniformly continuous. In paricular, for a fixed $\varepsilon > 0$ there exists $\delta > 0$ such that $|\mathbf{G}(s)-\mathbf{G}(\tilde{s})| < \varepsilon$ for $s, \tilde{s} \in [t-\delta, t+\delta]$. For $0 < h < \delta$ it folows $[t]_h, [t]_h+h \in [t-\delta, t+\delta]$, and so

$$\lim_{h\to 0+} |(\mathcal{P}_h\mathbf{G})(t) - \mathbf{G}(t)| \leq \lim_{h\to 0+} \frac{1}{h}\int_{[t]_h}^{[t]_h+h} |\mathbf{G}(s) - \mathbf{G}(t)|\,ds \leq \varepsilon.$$

But this yields

$$\lim_{h\to 0+} |(\mathcal{P}_h\mathbf{G})(t) - \mathbf{G}(t)| = 0$$

since ε is arbitrary small.

Now suppose $\mathbf{G}$ is not continuous at t, but it has finite left and right limits at t. If h is such that $[t]_h < t < [t]_h + h$, then

$$\begin{aligned}
&|(\mathcal{P}_h\mathbf{G})(t) - \mathbf{G}(t)| \\
&\quad = \frac{1}{h}\left|\int_{[t]_h}^{[t]_h+h} (\mathbf{G}(s) - \mathbf{G}(t))\,ds\right| \\
&\quad = \left|\frac{1}{t-[t]_h}\int_{[t]_h}^{t} (\mathbf{G}(s) - \mathbf{G}(t))\,ds\frac{t-[t]_h}{h}\right. \\
&\qquad \left. + \frac{1}{[t]_h+h-t}\int_{t}^{[t]_h+h} (\mathbf{G}(s) - \mathbf{G}(t))\,ds\frac{[t]_h+h-t}{h}\right| \\
&\quad \leq \frac{1}{t-[t]_h}\int_{[t]_h}^{t} |\mathbf{G}(s) - \mathbf{G}(t-)|\,ds + |\mathbf{G}(t-) - \mathbf{G}(t)| \\
&\qquad + \frac{1}{[t]_h+h-t}\int_{t}^{[t]_h+h} |\mathbf{G}(s) - \mathbf{G}(t+)|\,ds + |\mathbf{G}(t+) - \mathbf{G}(t)|.
\end{aligned}$$

If h is such that $t = [t]_h$, then

$$|(\mathcal{P}_h\mathbf{G})(t) - \mathbf{G}(t)| \leq \frac{1}{h}\int_{t}^{t+h} |\mathbf{G}(s) - \mathbf{G}(t+)|\,ds + |\mathbf{G}(t+) - \mathbf{G}(t)|.$$

Therefore in both cases we get statement (i), using an argument similar to that of the first case.

Clearly, $\mathbf{G}$ is constant on the intervals $[kh,(k+1)h)$, $k=0,1,\ldots$, therefore (ii) holds. Part (iii) is also obvious. □

Remark 1 Let $\mathbf{G}\in PC^1([0,\infty),\mathbb{R}^{n\times n})$, i.e., it is piecewise continuously differentiable, and $\mathbf{G}$ and its derivative have finite one-sided limits at the points of discontinuities, moreover suppose there exists $\bar{h}>0$ such that consecutive points of discontinuities of $\mathbf{G}$ have distance at least $\bar{h}$, then the proof of the previous lemma shows that for every $T>0$ there exists $L>0$ such that

$$|(\mathcal{P}_h\mathbf{G})(t)-\mathbf{G}(t)|\le Lh+|\mathbf{G}(t-)-\mathbf{G}(t)|+|\mathbf{G}(t+)-\mathbf{G}(t)|,\quad t\in[0,T],\quad 0<h<\bar{h}.$$

3.2 Semi-discretization

Consider again the delay system

$$\dot{\mathbf{x}}(t)=\mathbf{A}(t)\mathbf{x}(t)+\sum_{j=1}^{r}\mathbf{R}_j(t)\mathbf{x}(t-\tau_j)+\int_{-\sigma}^{0}\mathbf{W}(\vartheta,t)\mathbf{x}(t+\vartheta)\,d\vartheta\,, \tag{23}$$

and an associated initial condition

$$\mathbf{x}(t)=\varphi(t),\qquad t\in[-\rho,0], \tag{24}$$

where $\rho:=\max\{\tau_1,\ldots,\tau_r,\sigma\}$.

We assume that

(H1) the matrix valued functions $\mathbf{A},\mathbf{R_j}\in PC([0,\infty),\mathbb{R}^{n\times n})$ $(j=1,\ldots,p)$, and the constants $\sigma,\tau_1,\ldots,\tau_r>0$.

(H2) The weight function $\mathbf{W}\colon[-\sigma,0]\times[0,\infty)\to\mathbb{R}^{n\times n}$ is such that

(i) $\mathbf{W}(\cdot,t)\colon[-\sigma,0]\to\mathbb{R}^{n\times n}$ is continuous for each $t\in[0,\infty)$,

(ii) $\mathbf{W}(\vartheta,\cdot)\colon[0,\infty)\to\mathbb{R}^{n\times n}$ is piecewise-continuous for each $\vartheta\in[-\sigma,0]$.

(H3) The initial function $\varphi\in C([-\rho,0],\mathbb{R}^n)$.

(H4) Functions $\mathbf{A},\mathbf{R_j}$ $(j=1,\ldots,p)$, and for each ϑ, $\mathbf{W}(\vartheta,\cdot)$ are T-periodic, i.e., $\mathbf{A}(t+T)=\mathbf{A}(t)$, $\mathbf{R}_j(t+T)=\mathbf{R}_j(t)$ and $\mathbf{W}(\vartheta,t+T)=\mathbf{W}(\vartheta,t)$ for $t\ge0$, $\vartheta\in[-\sigma,0]$ and $j=1,\ldots,r$.

For a fixed positive integer m we define the discretization parameter $h = \sigma/m$, and consider the approximating equation corresponding to (23)

$$\begin{aligned}\dot{\mathbf{y}}_h(t) &= (\mathcal{P}_h\mathbf{A})(t)\mathbf{y}_h(t) + \sum_{j=1}^{r}(\mathcal{P}_h\mathbf{R}_j)(t)\mathbf{y}_h(\langle t\rangle_h - \langle\tau_j\rangle_h) \\ &\quad + \int_{-\sigma}^{0}(\mathcal{P}_h\mathbf{W})(\vartheta,t)\mathbf{y}_h(\langle t\rangle_h + \langle\vartheta\rangle_h)\,d\vartheta, \qquad t \geq 0, \end{aligned} \tag{25}$$

together with the associated initial condition

$$\mathbf{y}_h(t) = \varphi(t), \qquad t \in [-\rho, 0]. \tag{26}$$

Here we interpret $(\mathcal{P}_h\mathbf{W})$ as

$$(\mathcal{P}_h\mathbf{W})(\vartheta,t) = \frac{1}{h}\int_{[t]_h}^{[t]_h+h}\mathbf{W}(\vartheta,s)\,ds.$$

If $h < \tau_j$ for all j, then

$$\langle t\rangle_h - \langle\tau_j\rangle_h \leq t - \tau_j + h < t,$$

therefore (25) is a retarded equation.

Introduce the notations

$$\begin{aligned}\mathbf{A}_i &:= (\mathcal{P}_h\mathbf{A})(ih) = \frac{1}{h}\int_{ih}^{(i+1)h}\mathbf{A}(s)\,ds, \\ \mathbf{R}_{i,j} &:= (\mathcal{P}_h\mathbf{R}_j)(ih) = \frac{1}{h}\int_{ih}^{(i+1)h}\mathbf{R}_j(s)\,ds,\end{aligned}$$

and

$$\mathbf{W}_{i,j} := \int_{-jh}^{-(j-1)h}(\mathcal{P}_h\mathbf{W})(\vartheta,ih)\,d\vartheta = \frac{1}{h}\int_{-jh}^{-(j-1)h}\int_{ih}^{(i+1)h}\mathbf{W}(\vartheta,s)\,d\vartheta\,ds.$$

Suppose $t \in [ih,(i+1)h)$, i.e., $[t]_h = ih$, and let $m_j := [\tau_j]_h$. Then using these notations (25) can be written as

$$\dot{\mathbf{y}}_h(t) = \mathbf{A}_i\mathbf{y}_h(t) + \sum_{j=1}^{r}\mathbf{R}_{i,j}\mathbf{y}_h(ih - m_jh) + \sum_{j=1}^{m}\mathbf{W}_{i,j}\mathbf{y}_h(ih - jh + h).$$

If we introduce

$$\mathbf{y}_i := \mathbf{y}_h(ih), \quad i \in \mathbb{Z}, \quad ih \geq -\rho,$$

then we get

$$\dot{\mathbf{y}}_h(t) = \mathbf{A}_i\mathbf{y}_h(t) + \sum_{j=1}^{r}\mathbf{R}_{i,j}\mathbf{y}_{i-m_j} + \sum_{j=1}^{m}\mathbf{W}_{i,j}\mathbf{y}_{i-j+1}, \quad ih \leq t < (i+1)h,\ i = 0,1,\ldots. \tag{27}$$

Clearly, (27) has a unique solution defined for all $t \geq 0$. We refer the reader for more details on the computation of the solution of (27) to [8].

3.3 Convergence of the scheme

We now show in the next theorem that the solution of initial value problem (25)-(26) approximate that of (23)-(24).

Theorem 1 *Assume (H1)–(H3), then the solution of (25)-(26) approximate the solution of (23)-(24) uniformly on compact time intervals as $h \to 0+$ (or equivalently, $m \to \infty$), i.e., for every $S > 0$*

$$\lim_{h\to 0+} \max_{0\le t\le S} |\mathbf{x}(t) - \mathbf{y}_h(t)| = 0.$$

Proof Integrating (23) and (25) from 0 to t, respectively, we get

$$\mathbf{x}(t) = \varphi(0) + \int_0^t \mathbf{A}(u)\mathbf{x}(u)\,du + \sum_{j=1}^{r}\int_0^t \mathbf{R}_j(u)\mathbf{x}(u-\tau_j)\,du + \int_0^t\int_{-\sigma}^{0} \mathbf{W}(\vartheta,u)\mathbf{x}(u+\vartheta)\,d\vartheta du,$$

and

$$\begin{aligned}\mathbf{y}_h(t) &= \varphi(0) + \int_0^t (\mathcal{P}_h\mathbf{A})(u)\mathbf{y}_h(u)\,du + \sum_{j=1}^{r}\int_0^t (\mathcal{P}_h\mathbf{R}_j)(u)\mathbf{y}_h(\langle u\rangle_h - \langle\tau_j\rangle_h)\,du \\ &\quad + \int_0^t\int_{-\sigma}^{0} (\mathcal{P}_h\mathbf{W})(\vartheta,u)\mathbf{y}_h(\langle u\rangle_h + \langle\vartheta\rangle_h)\,d\vartheta\,du.\end{aligned}$$

Therefore simple manipulations give

$$\begin{aligned}&|\mathbf{x}(t) - \mathbf{y}_h(t)| \\ &\quad\le \alpha_h(t) + \int_0^t |(\mathcal{P}_h\mathbf{A})(s)||\mathbf{x}(u) - \mathbf{y}_h(u)|\,du \\ &\qquad + \sum_{j=1}^{r}\int_0^t |(\mathcal{P}_h\mathbf{R}_j)(u)||\mathbf{x}(\langle u\rangle_h - \langle\tau_j\rangle_h) - \mathbf{y}_h(\langle u\rangle_h - \langle\tau_j\rangle_h)|\,du \\ &\qquad + \int_0^t\int_{-\sigma}^{0} |(\mathcal{P}_h\mathbf{W})(\vartheta,u)||\mathbf{x}(\langle u\rangle_h + \langle\vartheta\rangle_h) - \mathbf{y}_h(\langle u\rangle_h + \langle\vartheta\rangle_h)|\,d\vartheta\,du, \quad (28)\end{aligned}$$

where

$$\begin{aligned}\alpha_h(t) &:= \int_0^t |\mathbf{A}(u) - (\mathcal{P}_h\mathbf{A})(u)||\mathbf{x}(u)|\,du + \sum_{j=1}^{r}\int_0^t |\mathbf{R}_j(u) - (\mathcal{P}_h\mathbf{R}_j)(u)||\mathbf{x}(u-\tau_j)|\,du \\ &\quad + \sum_{j=1}^{r}\int_0^t |(\mathcal{P}_h\mathbf{R}_j)(u)||\mathbf{x}(u-\tau_j) - \mathbf{x}(\langle u\rangle_h - \langle\tau_j\rangle_h)|\,du \\ &\quad + \int_0^t\int_{-\sigma}^{0} |\mathbf{W}(\vartheta,u) - (\mathcal{P}_h\mathbf{W})(\vartheta,u)||\mathbf{x}(u+\vartheta)|\,d\vartheta\,du \\ &\quad + \int_0^t\int_{-\sigma}^{0} |(\mathcal{P}_h\mathbf{W})(\vartheta,u)||\mathbf{x}(u+\vartheta) - \mathbf{x}(\langle u\rangle_h + \langle\vartheta\rangle_h)|\,d\vartheta\,du.\end{aligned}$$

Note that $\alpha_h(t)$ is a monotone increasing function in t. It follows from (21), Lemma 1 (i), (iii), the boundedness of the functions $\mathbf{A}$, $\mathcal{P}_h\mathbf{A}$, $\mathbf{R}_j$, $\mathcal{P}_h\mathbf{R}_j$, $\mathbf{W}$, $\mathcal{P}_h\mathbf{W}$, and $\mathbf{x}$ over compact time intervals, and the Lebesgue's Dominated Convergence Theorem, that

$$\lim_{h\to 0+} \alpha_h(S) = 0, \qquad S \geq 0. \tag{29}$$

We introduce

$$w_h(t) := \max\{|\mathbf{x}(s) - \mathbf{y}_h(s)|\colon\ 0 \leq s \leq t\}.$$

Then $w_h(t)$ is a monotone increasing function of t, so (28) implies

$$|\mathbf{x}(t) - \mathbf{y}_h(t)| \leq \alpha_h(t) + \int_0^t \beta_h(u) w_h(u)\, du$$

where

$$\beta_h(u) := |(\mathcal{P}_h\mathbf{A})(u)| + \sum_{j=1}^{r} |(\mathcal{P}_h\mathbf{R}_j)(u)| + \int_{-\sigma}^{0} |(\mathcal{P}_h\mathbf{W})(\vartheta, u)|\, d\vartheta.$$

Then the monotonicity of α_h and w_h and (28) yield for $s < t$

$$|\mathbf{x}(s) - \mathbf{y}_h(s)| \leq \alpha_h(s) + \int_0^s \beta_h(u) w_h(u)\, du \leq \alpha_h(t) + \int_0^t \beta_h(u) w_h(u)\, du, \qquad 0 \leq s < t,$$

therefore

$$w_h(t) \leq \alpha_h(t) + \int_0^t \beta_h(u) w_h(u)\, du, \qquad t \geq 0.$$

Hence, using Growall's inequality, we obtain

$$|\mathbf{x}(t) - \mathbf{y}_h(t)| \leq w_h(t) \leq \alpha_h(t) e^{\int_0^t \beta_h(u)\, du}, \qquad t \geq 0.$$

Then the statement of the theorem follows from (29), since β_h is bounded by a constant independent of h over $[0, S]$. □

We comment that in the previous proof the particular form of the discretization operator $\mathcal{P}_h$ and the function $\langle t \rangle_h$ was not important, the proof uses only the properties of $\mathcal{P}_h$ summarized in Lemma 1 and relation (21).

Remark 2 If in addition to (H1)–(H3) we assume

$$\mathbf{A}, \mathbf{R}_j, \mathbf{W}(\vartheta, \cdot) \in PC^1([0, \infty), \mathbb{R}^{n\times n}), \quad (j = 1, \ldots, p, \quad \vartheta \in [-\sigma, 0]),$$

and the distance between consecutive points of discontinuities of all functions is at least $\bar{h} > 0$, and $\varphi \in C^1([-\rho, 0], \mathbb{R}^n)$, then it is easy to show, using Remark 1, that the convergence in the statement of Theorem 1 is first order, i.e., for every $S > 0$ there exists $M > 0$ such that

$$\max_{0\leq t\leq S} |\mathbf{x}(t) - \mathbf{y}_h(t)| \leq Mh, \qquad 0 < h < \bar{h}.$$

3.4 Preservation of Asymptotic Stability

The next theorem shows that the asymptotic stability of (23) is preserved under the semi-discretization (25). Such issue was studied for several classes of functional differential equations in [17] and [18] using spline based schemes. For the full-discretization method we refer to [19] and [20] for related works.

Theorem 2 *Assume (H1)–(H4) and that the trivial solution of (23) is asymptotically stable. Then there exists $h_0 > 0$ such that the trivial solution of (25) is asymptotically stable for all $0 < h < h_0$.*

Proof We associate initial conditions (24) and (26) (with the same initial function φ) to (23) and (25), respectively. The fundamental matrix solution of (23) is the $n \times n$ matrix solution of the initial value problem

$$\dot{\mathbf{V}}(t,s) = \mathbf{A}(t)\mathbf{V}(t,s) + \sum_{j=1}^{r} \mathbf{R}_j(t)\mathbf{V}(t-\tau_j,s) + \int_{-\sigma}^{0} \mathbf{W}(\vartheta,t)\mathbf{V}(t+\vartheta,s)\,d\vartheta, \quad t \geq 0, \tag{30}$$

$$\mathbf{V}(t,s) = \begin{cases} \mathbf{I}, & t = s, \\ \mathbf{0}, & t < s, \end{cases} \tag{31}$$

where $\mathbf{I}$ is the identity and $\mathbf{0}$ is the zero matrix. Since (23) is periodic, it is known (see, e.g., [21]) that the trivial solution of (23) is asymptotically stable, if and only if it is exponentially stable, i.e., there exist constants $K \geq 1$ and $\alpha \geq 0$ such that

$$|\mathbf{x}(t)| \leq Ke^{-\alpha t}\|\varphi\|, \qquad t \geq 0, \tag{32}$$

where $\|\varphi\| = \max\{|\varphi(t)| \colon t \in [-\rho, 0]\}$. This is also equivalent to that the fundamental solution of (23) is exponentially bounded, i.e., there exist constants $K_0, \alpha_0 > 0$ such that

$$|\mathbf{V}(t,s)| \leq K_0 e^{-\alpha_0(t-s)}, \qquad t \geq s. \tag{33}$$

We can rewrite (25) as

$$\dot{\mathbf{y}}_h(t) = \mathbf{A}(t)\mathbf{y}_h(t) + \sum_{j=1}^{r} \mathbf{R}_j(t)\mathbf{y}_h(t-\tau_j) + \int_{-\sigma}^{0} \mathbf{W}(\vartheta,t)\mathbf{y}_h(t+\vartheta)\,d\vartheta + \gamma_h(t) + \delta_h(t),$$

where

$$\begin{aligned} \gamma_h(t) &= \Big((\mathcal{P}_h\mathbf{A})(t) - \mathbf{A}(t)\Big)\mathbf{y}_h(t) + \sum_{j=1}^{r}\Big((\mathcal{P}_h\mathbf{R}_j)(t) - \mathbf{R}_j(t)\Big)\mathbf{y}_h(t-\tau_j) \\ &\quad + \int_{-\sigma}^{0}\Big((\mathcal{P}_h\mathbf{W})(\vartheta,t) - \mathbf{W}(\vartheta,t)\Big)\mathbf{y}_h(t+\vartheta)\,d\vartheta, \qquad t \geq 0, \end{aligned}$$

and

$$\begin{aligned}\delta_h(t) &= \sum_{j=1}^{r}(\mathcal{P}_h\mathbf{R}_j)(t)\Big(\mathbf{y}_h(\langle t\rangle_h-\langle\tau_j\rangle_h)-\mathbf{y}_h(t-\tau_j)\Big)\\ &\quad+\int_{-\sigma}^{0}(\mathcal{P}_h\mathbf{W})(\vartheta,t)\Big(\mathbf{y}_h(\langle t\rangle_h+\langle\vartheta\rangle_h)-\mathbf{y}_h(t+\vartheta)\Big)\,d\vartheta,\qquad t\ge 0.\end{aligned}$$

Therefore, (25) can be considered as a perturbation of (23) with $\gamma_h+\delta_h$, hence the variation of constants formula (see, e.g., [21]) yields

$$\mathbf{y}_h(t)=\mathbf{x}(t)+\int_0^t\mathbf{V}(t,s)(\gamma_h(s)+\delta_h(s))\,ds,\qquad t\ge 0. \tag{34}$$

We prove the theorem in two steps: first we show that $\mathbf{y}_h$ will be bounded on $[0,\infty)$ for small h, then prove that $\mathbf{y}_h(t)\to 0$ as $t\to\infty$ for small h.

1. We estimate both perturbation terms, $\int_0^t\mathbf{V}(t,s)\gamma_h(s)\,ds$ and $\int_0^t\mathbf{V}(t,s)\delta_h(s)\,ds$. Let $z_h(t)=\max\{|\mathbf{y}_h(s)|\colon -\rho\le s\le t\}$.

To estimate $\int_0^t\mathbf{V}(t,s)\gamma_h(s)\,ds$ we first introduce $m=[\frac{t}{T}]$. Then (33), the definition of z_h, relation $mT\le t<(m+1)T$ and simple estimates yield

$$\begin{aligned}&\left|\int_0^t\mathbf{V}(t,s)\gamma_h(s)\,ds\right|\\ &\quad\le\int_0^t|\mathbf{V}(t,s)|\Big(\Big|(\mathcal{P}_h\mathbf{A})(s)-\mathbf{A}(s)\Big||\mathbf{y}_h(s)|+\sum_{j=1}^{r}\Big|(\mathcal{P}_h\mathbf{R}_j)(s)-\mathbf{R}_j(s)\Big||\mathbf{y}_h(s-\tau_j)|\\ &\qquad+\int_{-\sigma}^{0}\Big|(\mathcal{P}_h\mathbf{W})(\vartheta,s)-\mathbf{W}(\vartheta,s)\Big||\mathbf{y}_h(s+\vartheta)|\,d\vartheta\Big)ds\\ &\quad\le K_0e^{-\alpha_0t}\int_0^t e^{\alpha_0s}\Big(\Big|(\mathcal{P}_h\mathbf{A})(s)-\mathbf{A}(s)\Big|+\sum_{j=1}^{r}\Big|(\mathcal{P}_h\mathbf{R}_j)(s)-\mathbf{R}_j(s)\Big|\\ &\qquad+\int_{-\sigma}^{0}\Big|(\mathcal{P}_h\mathbf{W})(\vartheta,s)-\mathbf{W}(\vartheta,s)\Big|\,d\vartheta\Big)ds\cdot z_h(t)\\ &\quad\le K_0e^{-\alpha_0mT}\sum_{k=0}^{m}\int_{kT}^{(k+1)T}e^{\alpha_0s}\Big(\Big|(\mathcal{P}_h\mathbf{A})(s)-\mathbf{A}(s)\Big|+\sum_{j=1}^{r}\Big|(\mathcal{P}_h\mathbf{R}_j)(s)-\mathbf{R}_j(s)\Big|\\ &\qquad+\int_{-\sigma}^{0}\Big|(\mathcal{P}_h\mathbf{W})(\vartheta,s)-\mathbf{W}(\vartheta,s)\Big|\,d\vartheta\Big)ds\cdot z_h(t),\qquad t\ge 0.\end{aligned}$$

Therefore, using the T-periodicity of the functions $\mathbf{A}$, $\mathcal{P}_h\mathbf{A}$, $\mathbf{R}_j$, $\mathcal{P}_h\mathbf{R}_j$, $\mathbf{W}(\vartheta,\cdot)$, and $\mathcal{P}_h\mathbf{W}(\vartheta,\cdot)$,

$$\begin{aligned}
&\left|\int_0^t \mathbf{V}(t,s)\gamma_h(s)\,ds\right| \\
&\quad\le\ K_0e^{-\alpha_0 mT}\sum_{k=0}^{m} e^{\alpha_0(k+1)T}\int_0^T\Big(\Big|(\mathcal{P}_h\mathbf{A})(s)-\mathbf{A}(s)\Big|+\sum_{j=1}^{r}\Big|(\mathcal{P}_h\mathbf{R}_j)(s)-\mathbf{R}_j(s)\Big| \\
&\qquad+\int_{-\sigma}^{0}\Big|(\mathcal{P}_h\mathbf{W})(\vartheta,s)-\mathbf{W}(\vartheta,s)\Big|\,d\vartheta\Big)ds\cdot z_h(t) \\
&\quad\le\ A_h z_h(t), \qquad t\ge 0,
\end{aligned} \tag{35}$$

where

$$\begin{aligned}
A_h\ =\ &\frac{K_0e^{2\alpha_0 T}}{e^{\alpha_0 T}-1}\int_0^T\Big(\Big|(\mathcal{P}_h\mathbf{A})(s)-\mathbf{A}(s)\Big|+\sum_{j=1}^{r}\Big|(\mathcal{P}_h\mathbf{R}_j)(s)-\mathbf{R}_j(s)\Big| \\
&+\int_{-\sigma}^{0}\Big|(\mathcal{P}_h\mathbf{W})(\vartheta,s)-\mathbf{W}(\vartheta,s)\Big|\,d\vartheta\Big)ds.
\end{aligned}$$

It follows from Lemma 1 and the Lebesgue's Dominated Convergence Theorem that $A_h\to 0$ as $h\to 0+$.

To estimate $\int_0^t \mathbf{V}(t,s)\delta_h(s)\,ds$ we first introduce some additional notation. Assumptions (H1)–(H4) imply that there exist constants $M_0, M_1, \dots, M_{r+1} > 0$ such that

$$|\mathbf{A}(t)|\le M_0,\quad |\mathbf{R}_j(t)|\le M_j,\quad (j=1,\dots,r)\quad |\mathbf{W}(\vartheta,t)|\le\frac{M_{r+1}}{\sigma},\quad t\ge 0,\ \vartheta\in[-\sigma,0],$$

and hence, by Lemma 1,

$$|(\mathcal{P}_h\mathbf{A})(t)|\le M_0,\quad |(\mathcal{P}_h\mathbf{R}_j)(t)|\le M_j,\quad (j=1,\dots,r)\quad |(\mathcal{P}_h\mathbf{W})(\vartheta,t)|\le\frac{M_{r+1}}{\sigma},$$

for $t\ge 0,\ \vartheta\in[-\sigma,0]$. Using (25) we get for $t\ge\rho$

$$\begin{aligned}
\delta_h(t)\ =\ &\sum_{j=1}^{r}(\mathcal{P}_h\mathbf{R}_j)(t)\int_{t-\tau_j}^{\langle t\rangle_h-\langle\tau_j\rangle_h}\dot{\mathbf{y}}_h(u)\,du+\int_{-\sigma}^{0}(\mathcal{P}_h\mathbf{W})(\vartheta,t)\int_{t+\vartheta}^{\langle t\rangle_h+\langle\vartheta\rangle_h}\dot{\mathbf{y}}_h(u)\,du\,d\vartheta \\
=\ &\sum_{j=1}^{r}(\mathcal{P}_h\mathbf{R}_j)(t)\int_{t-\tau_j}^{\langle t\rangle_h-\langle\tau_j\rangle_h}\Big((\mathcal{P}_h\mathbf{A})(u)\mathbf{y}_h(u)+\sum_{k=1}^{r}(\mathcal{P}_h\mathbf{R}_k)(u)\mathbf{y}_h(\langle u\rangle_h-\langle\tau_k\rangle_h) \\
&+\int_{-\sigma}^{0}(\mathcal{P}_h\mathbf{W})(\vartheta,u)\mathbf{y}_h(\langle u\rangle_h+\langle\vartheta\rangle_h)\,d\vartheta\Big)du \\
&+\int_{-\sigma}^{0}(\mathcal{P}_h\mathbf{W})(\vartheta,t)\int_{t+\vartheta}^{\langle t\rangle_h+\langle\vartheta\rangle_h}\Big((\mathcal{P}_h\mathbf{A})(u)\mathbf{y}_h(u)+\sum_{k=1}^{r}(\mathcal{P}_h\mathbf{R}_k)(u)\mathbf{y}_h(\langle u\rangle_h-\langle\tau_k\rangle_h) \\
&+\int_{-\sigma}^{0}(\mathcal{P}_h\mathbf{W})(\lambda,u)\mathbf{y}_h(\langle u\rangle_h+\langle\lambda\rangle_h)\,d\lambda\Big)du\,d\vartheta.
\end{aligned} \tag{36}$$

Then relations $|\langle t\rangle_h - \langle \tau_k\rangle_h - (t-\tau_k)| \le h$ and $|\langle t\rangle_h + \langle \vartheta\rangle_h - (t+\vartheta)| \le h$, and the definitions of $M_0, \dots, M_{r+1}$ imply

$$|\delta_h(t)| \le h\sum_{j=1}^{r} M_j\Big(\sum_{k=0}^{r+1} M_k\Big) z_h(t) + hM_{r+1}\Big(\sum_{k=0}^{r+1} M_k\Big) z_h(t) \le h\Big(\sum_{k=0}^{r+1} M_k\Big)^2 z_h(t), \quad t \ge \rho,$$

and

$$|\delta_h(t)| \le \sum_{k=1}^{r+1} M_k 2 z_h(\rho), \qquad t \in [0,\rho].$$

Since, by Theorem 1 and (32),

$$|\mathbf{y}_h(t)| \le |\mathbf{x}(t)| + |\mathbf{y}_h(t) - \mathbf{x}(t)| \le K\|\varphi\| + 1, \qquad t \in [0,\rho], \quad 0 \le h \le h_1,$$

we get

$$|\delta_h(t)| \le \sum_{k=1}^{r+1} M_k 2(K\|\varphi\| + 1), \qquad t \in [0,\rho], \quad 0 \le h \le h_1.$$

Therefore, for $0 \le h \le h_1$,

$$\begin{aligned}\left|\int_0^t \mathbf{V}(t,s)\delta_h(s)\,ds\right| \le{}& \left|\int_0^\rho \mathbf{V}(t,s)\delta_h(s)\,ds\right| + \left|\int_\rho^t \mathbf{V}(t,s)\delta_h(s)\,ds\right| \\ \le{}& \rho K_0 \sum_{k=1}^{r+1} M_k 2(K\|\varphi\|+1) + K_0\int_\rho^t e^{-\alpha_0(t-s)}\,ds\, h\Big(\sum_{k=0}^{r+1} M_k\Big)^2 z_h(t) \\ \le{}& B + Ch z_h(t), \qquad t \ge 0, \end{aligned} \tag{37}$$

where

$$B = \rho K_0 \sum_{k=1}^{r+1} M_k 2(K\|\varphi\|+1), \qquad C = \frac{K_0}{\alpha_0}\Big(\sum_{k=0}^{r+1} M_k\Big)^2.$$

Combining (34), (35) and (37) yields

$$|\mathbf{y}_h(t)| \le K\|\varphi\| + B + (A_h + Ch) z_h(t), \qquad t \ge 0,$$

and so, using $|\mathbf{y}_h(t)| \le \|\varphi\|$ and that the right hand side is monotone in t, we get

$$z_h(t) \le K\|\varphi\| + B + (A_h + Ch) z_h(t), \qquad t \ge 0.$$

If $0 < h_0 \le h_1$ is such that $A_h + Ch < 1$ for $0 < h \le h_0$, then

$$|\mathbf{y}_h(t)| \le z_h(t) \le \frac{K\|\varphi\| + B}{1 - A_h - Ch}, \qquad t \ge 0,$$

therefore the solutions of (25) are bounded on $[0,\infty)$.

2. Now we show that $\lim_{t\to 0} |\mathbf{y}_h(t)| = 0$. Consider again (34). Since $\lim_{t\to\infty} |\mathbf{x}(t)| = 0$, we get

$$\limsup_{t\to\infty} |\mathbf{y}_h(t)| \le \limsup_{t\to\infty} K_0 \int_0^t e^{-\alpha_0(t-s)}(|\gamma_h(s)| + |\delta_h(s)|)\,ds. \tag{38}$$

The second part on the right hand side can be estimated using Lemma 2.3 in [22], and (36) as follows

$$\begin{aligned}\limsup_{t\to\infty} K_0\int_0^t e^{-\alpha_0(t-s)}|\delta_h(s)|\,ds &\le K_0\int_0^\infty e^{-\alpha_0 t}\,dt\cdot\limsup_{t\to\infty}|\delta_h(t)|\\ &\le \frac{K_0}{\alpha_0}h\Big(\sum_{k=0}^{r+1}M_k\Big)^2\limsup_{t\to\infty}|\mathbf{y}_h(t)|. \qquad (39)\end{aligned}$$

The first part requires a more careful estimate, similar to the derivation of (35). Let $\varepsilon>0$ be fixed, then there exists such $N=N(\varepsilon,h)$ that $|\mathbf{y}_h(t)|\le\limsup_{t\to\infty}|\mathbf{y}_h(t)|+\varepsilon$ for $t\ge NT-\rho$. Let $m(t)=[t/T]$. Then

$$\begin{aligned}&\limsup_{t\to\infty}\int_0^t e^{-\alpha_0(t-s)}|\gamma_h(s)|\,ds\\ &\le \limsup_{t\to\infty}e^{-\alpha_0 t}\int_0^{NT}e^{\alpha_0 s}|\gamma_h(s)|\,ds+\limsup_{t\to\infty}\int_{NT}^t e^{-\alpha_0(t-s)}|\gamma_h(s)|\,ds\\ &\le \limsup_{t\to\infty}e^{-\alpha_0 m(t)T}\sum_{k=N}^{m(t)}\int_{kT}^{(k+1)T}e^{\alpha_0 s}\Big(\Big|(\mathcal{P}_h\mathbf{A})(s)-\mathbf{A}(s)\Big|+\sum_{j=1}^r\Big|(\mathcal{P}_h\mathbf{R}_j)(s)-\mathbf{R}_j(s)\Big|\\ &\qquad+\int_{-\sigma}^0\Big|(\mathcal{P}_h\mathbf{W})(\vartheta,s)-\mathbf{W}(\vartheta,s)\Big|\,d\vartheta\Big)ds\,(\limsup_{t\to\infty}|\mathbf{y}_h(t)|+\varepsilon)\\ &\le \limsup_{t\to\infty}e^{-\alpha_0 m(t)T}\sum_{k=N}^{m(t)}e^{\alpha_0(k+1)T}\int_0^T\Big(\Big|(\mathcal{P}_h\mathbf{A})(s)-\mathbf{A}(s)\Big|+\sum_{j=1}^r\Big|(\mathcal{P}_h\mathbf{R}_j)(s)-\mathbf{R}_j(s)\Big|\\ &\qquad+\int_{-\sigma}^0\Big|(\mathcal{P}_h\mathbf{W})(\vartheta,s)-\mathbf{W}(\vartheta,s)\Big|\,d\vartheta\Big)ds\,(\limsup_{t\to\infty}|\mathbf{y}_h(t)|+\varepsilon)\\ &\le \frac{A_h}{K_0e^{2\alpha_0 T}}(\limsup_{t\to\infty}|\mathbf{y}_h(t)|+\varepsilon).\end{aligned}$$

Since this estimate holds for any ε, it follows that

$$\limsup_{t\to\infty}\int_0^t e^{-\alpha_0(t-s)}|\gamma_h(s)|\,ds\le\frac{A_h}{K_0e^{2\alpha_0 T}}\limsup_{t\to\infty}|\mathbf{y}_h(t)|. \qquad (40)$$

Combining (38), (39) and (40) we get

$$\limsup_{t\to\infty}|\mathbf{y}_h(t)|\le\left(\frac{A_h}{e^{2\alpha_0 T}}+\frac{K_0}{\alpha_0}h\Big(\sum_{k=0}^{r+1}M_k\Big)^2\right)\limsup_{t\to\infty}|\mathbf{y}_h(t)|,$$

which concludes the proof, since for small enough h, the coefficient on the right hand side is less than 1, therefore $\limsup_{t\to\infty}|\mathbf{y}_h(t)|=\lim_{t\to\infty}|\mathbf{y}_h(t)|=0$. □

Remark 3 If in addition to (H1)–(H4) we suppose the assumptions listed in Remark 2, then it is easy to find a $D>0$ such that $A_h\le Dh$, therefore the constant, h_0, in the statement of Theorem 2 can be given explicitly.

4 Acknowledgement

This research was supported in part by the Magyary Zoltán Postdoctoral Fellowship of Foundation for Hungarian Higher Education and Research (T.I.), by the Hungarian National Science Foundation under grants no. OTKA T043368 (G.S.), T046929 (F.H.) and F047318 (T.I.) and by the Domus Hungarica Scientiarium et Artium Foundation (J.T.).

5 References

[1] V. Volterra, Sur la Theorie Mathematique des Phenomenes Hereditares, *Journal de Mathématiques Pures et Appliqués*, **7** (1928), pp. 149-192.

[2] B. von Schlippe, R. Dietrich, Shimmying of a Pneumatic Wheel, Lilienthal-Gesellschaft für Luftfahrtforschung, *Bericht*, **140** (1941), translated for the *AAF* in 1947 by Meyer & Company, pp. 125-160.

[3] N., Minorsky, Selfexcited Oscillations in Dynamical Systems Possessing Retarded Actions, *Journal of Applied Mechanics*, **9** (1942), pp. 65-71.

[4] G. Stépán, *Retarded Dynamical Systems*, Longman, Harlow, 1989.

[5] T. Insperger, B. P. Mann, G. Stépán, P. V. Bayly, Stability of up-milling and down-milling, Part 1: Alternative analytical methods, International Journal of Machine Tools and Manufacture, **43**(1) (2003), pp. 25-34.

[6] G. Stépán, G. Haller, Quasiperiodic oscillations in robot dynamics, *Nonlinear Dynamics*, **8** (1995), pp. 513-528.

[7] S. A. Campbell, S. Ruan, J. Wei, Qualitative analysis of a neural network model with multiple time delays, *International Journal of Bifurcation and Chaos*, **9**(8) (1999), pp. 1585-1595.

[8] T. Insperger, G. Stépán, Semi-discretization method for delayed systems, *International Journal for Numerical Methods in Engineering*, **55**(5) (2002), pp. 503-518.

[9] T. Insperger, G. Stépán, Stability analysis of turning with periodic spindle speed modulation via semi-discretization, *Journal of Vibration and Control*, in press (2004).

[10] L. L. Kovács, G. Stépán, T. Insperger, Outer-loop force control of industrial robots, in *Proceedings of the 11th World Congress in Mechanism and Machine*

Science (ed.: Tian Huang), Tianjin, China (2004) China Machinery Press, pp. 1746-1750.

[11] O. Elbeyli, J. Q. Sun, G. Ünal, A Semi-Discretization Method for Delayed Stochastic Systems, *Communication in Nonlinear Science and Numerical Simulation*, **10**(1) (2005), pp. 85-94.

[12] T. Insperger, G. Stépán, Updated semi-discretization method for periodic delay-differential equations with discrete delay, *International Journal of Numerical Methods in Engineering*, **61**(1) (2004) pp. 117-141.

[13] O. Elbeyly, J. Q. Sun, On the semi-discretization method for feedback control design of linear systems with time delay, *Journal of Sound and Vibration*, **273**(1-2) (2004), pp. 429-440.

[14] I. Győri, On approximation of the solutions of delay differential equations by using piecewise constant arguments, *Internat. J. of Math. & Math. Sci.*, **14**(1) (1991), pp. 111-126 .

[15] I. Győri, F. Hartung, J. Turi, Numerical approximations for a class of differential equations with time- and state-dependent delays, *Applied Mathematics Letters*, **8**(6) (1995), pp. 19-24.

[16] V. Lakshmikantham, D. Trigiante, *Theory of Difference Equations, Numerical Methods and Applications*, Academic Press, London, 1988.

[17] R. H. Fabiano, J. Turi, Preservation of stability under approximation for a neutral FDE, *Dynam. Contin. Discrete Impuls. Systems* **5** (1999), pp. 351-364.

[18] R. H. Fabiano, Renorming for stability and approximation of linear systems: Examples, *Math. Comput. Modelling* **33** (2001), pp. 159-172.

[19] K. L. Cooke, I. Győri, Numerical approximation of the solutions of delay differential equations on an infinite interval using piecewise constant arguments, *Comput. Math. Appl.*, **28**(1-3) (1994), pp. 81-92.

[20] I. Győri, F. Hartung, Numerical approximation of neutral differential equations on infinite interval, *J. Difference Equ. Appl.* **8**(11) (2002), pp. 983-999.

[21] J. K. Hale, Verduyn Lunel, S. M., *Introduction to Functional Differential Equations*, Spingler-Verlag, New York, 1993.

[22] I. Győri, Global attractivity in delay differential equations using a mixed monotone technique, *J. Math. Anal. Appl.* **152** (1990) 131-155.

List of Figures

1 Modeling the entering end exiting teeth in the milling process 4
2 Graph of $K(t)$ 5
3 Semi-discretized simulation for (2) with different step sizes 6
4 Fully-discretized simulation for (2) for different step sizes 7
5 Semi-discretized stability charts for (2) for different step sizes 8
6 Fully-discretized stability charts for (2) for different step sizes 10
7 The graph of $\langle t \rangle_h$ 11